Uplink-Based Framework for Control Plane Applications in 5G mmWave Cellular Networks

Marco Giordani[†], **Marco Mezzavilla**[◇], **Sundeep Rangan**[◇], **Michele Zorzi**[†]

[†] University of Padova, Italy [◇]NYU Wireless, Brooklyn, NY, USA

emails: {giordani, zorzi}@dei.unipd.it, {mezzavilla, srangan}@nyu.edu

Abstract

The millimeter wave (mmWave) frequencies offer the potential of orders of magnitude increases in capacity for next-generation cellular systems. However, links in mmWave networks are susceptible to blockage and may suffer from rapid variations in quality. Connectivity to multiple cells – in the mmWave and in the traditional frequencies – is considered essential for robust connectivity. One of the challenges in supporting multi-connectivity in mmWaves is the requirement for the network to track the direction of each link in addition to its power and timing. To address this challenge, this paper proposes a novel uplink measurement system based on (i) the UE transmitting sounding signals in directions that sweep the angular space, (ii) the mmWave cells measuring the instantaneous received signal strength along with its variance to capture the dynamics and the reliability of a channel/direction and, finally, (iii) a centralized controller making scheduling decisions based on the mmWave cell reports and transmitting the decisions either via a mmWave cell or a conventional LTE cell (when the paths are not available). We argue that the proposed scheme enables fair and robust cell selection, in addition to efficient and periodical tracking of the user, in the presence of the channel variability expected at mmWaves.

Index Terms

5G, millimeter wave, multi-connectivity, initial access, handover, blockage, beam tracking.

I. Introduction

The millimeter wave (mmWave) bands – roughly above 10 GHz – have attracted considerable attention for meeting the ever more demanding performance requirements of micro and picocellular networks [1]. These frequencies offer much more bandwidth than current cellular systems in the congested microwave bands below 3 GHz, and initial capacity estimates have suggested that mmWave networks can offer orders of magnitude greater capacity than 4G systems [2].

However, the increased carrier frequency of mmWave systems makes the propagation conditions more demanding than at the lower frequencies traditionally used for wireless services, especially in terms of robustness. MmWave signals are blocked by many common building materials such as brick, and the human body can also significantly attenuate signals in the mmWave range [3]. Thus, the communication quality between the user equipment (UE) and any one cell can be highly variable as the movement of obstacles or even the changing position of the body relative to the mobile device can lead to rapid drops in signal strength. One likely key feature of mmWave cellular networks that can improve robustness is *multi-connectivity* (MC) [4], which enables each UE to maintain multiple possible signal paths to different cells so that drops in one link can be overcome by switching data paths. Multi-connectivity can be both among multiple 5G mmWave cells as well as between 5G mmWave cells and traditional 4G cells below 3 GHz. Mobiles with such 4G/5G multi-connectivity can benefit from both the mmWave channels with high capacities, as well as the more robust, but lower capacity, microwave channels, thereby opening up new ways of solving capacity issues, as well as new of providing good mobile network performance and robustness [5].

This paper addresses one of the key challenges in supporting multi-connectivity in heterogeneous networks (HetNets) with mmWave cells, namely directional multi-cell channel tracking and measurement reports. Channel tracking and measurement reports are fundamental for cellular systems to properly perform a wide variety of control tasks including handover, path selection, and radio link failure (RLF) detection and recovery. However, while channel tracking and reporting is relatively straightforward in cellular systems at conventional frequencies, the mmWave bands present several significant limitations: (i) the high variability of the channel in each link due to blockage [6], [7]; (ii) the need to track multiple directions for each link [8]; and (iii) reports from the UE back to the cells must be made directional. To address these challenges, as an extension of our prior work [9], this paper proposes a *novel* multi-cell measurement reporting system where each UE directionally broadcasts a sounding reference signal (SRS) in a time-varying direction that continuously sweeps the angular space. Each potential serving cell scans all its angular directions and monitors the strength of the received SRS along with its variance, to better capture the dynamics of the channel. A centralized controller (that can be identified by a microwave base station) obtains complete directional knowledge from all the potential cells in the network to make the optimal serving cell selection and scheduling decision.

Unlike in traditional LTE channel aggregation, the proposed system is based on the channel quality of uplink (UL) rather than downlink (DL) signals. This eliminates the need for the UE to send measurement reports back to the network and thereby removes a possible point of failure in the control signaling path. Moreover, we show that if digital beamforming or beamforming with multiple analog streams is available at the mmWave cell, then the directional scan time can be dramatically reduced when using UL-based measurements.

Additionally, in the case when the mmWave links are not available, the network is able to send the scheduling and serving cell decisions over the legacy cells, since microwave bands are almost transparent to obstacles. Such multi-frequency control signaling can be exploited to implement more robust and stable resource allocation and network management.

We also show that the proposed UL scheme can also be leveraged for fast initial access. Initial access, mobility management and handover are fundamental MAC layer functions that specify how a UE should connect to the network and preserve its connectivity. For example, frequent handover, even for fixed UEs, is a potential drawback of mmWave systems due to their vulnerability to random obstacles, which is not the case in LTE. Dense deployments of short range BSs, as foreseen in mmWave cellular networks, may exacerbate frequent handovers between adjacent BSs [10]. We argue that the proposed UL-based framework can be used to address some of these important 5G control plane challenges that arise when dealing with the mmWave frequency bands. In particular, we show that the proposed scheme enables robust and efficient handover, fast and fair initial cell selection and fast and effective reaction to blockage.

The remainder of the paper is organized as follows. In Section II we review some of the most important contributions related to MC in mmWave cellular systems. In Section III, we describe the multi-cell measurement procedure. In Section IV, we show how our framework can be used towards designing better control strategies. In Section V we present the parameters used to carry out the simulations, while Section VI provides some results related to the control applications presented in the paper. Finally, we conclude this work and we list some future research steps in Section VII.

II. Related Work

Channel estimation is relatively straightforward in LTE [11]. However, in addition to the rapid variations of the channel, transmissions in mmWaves are expected to be directional, and thus the

network and UE must constantly monitor the direction of transmission of each potential link. Tracking changing directions can slow the rate at which the network can adapt and can be a major obstacle in providing robust service in the face of variable link quality. In addition, the UE and the base station (BS) may only be able to listen to one direction at a time, thus making it hard to receive the control signaling necessary to switch paths.

Dual-connectivity has been proposed in Release 12 of Long Term Evolution-Advance (LTE-A) [12]. This feature supports inter-frequency and intra-frequency connectivity as well as connectivity to different types of base stations (e.g., macro and pico base stations) [13]. However, these systems were designed for conventional frequencies and the directionality and variability of the channels present at mmWave frequencies is not addressed.

Some other previous works, such as [14], consider the bands under 6 GHz as the only control channel for 5G networks, to provide robustness against blockage and wider coverage range. However, high capacities can also be obtained just exploiting the mmWave frequencies. So, in [4], a multi-connectivity framework is proposed as a solution for mobility-related link failures and throughput degradation of cell-edge users, relying on the fact that the transmissions from cooperating cells are coordinated for both data and control signals.

The work in [15] assumes HetNet deployment of small cells and proposes that the control plane is handled centrally for small geographical areas whereas, for large geographical areas, distributed control should be used. However, the performance evaluation of small cells that use the same carrier frequency deployed over a relatively wider area has not yet been investigated.

In our previous work [9] we argued that the proposed multi-connectivity multi-cell scheme enables efficient and highly adaptive cell selection in the presence of the mmWave channel variability. As an extension of such a work, this paper aims at defining an UL framework for implementing fair and robust control applications in upcoming 5G networks.

III. Procedure Description

In the proposed framework, illustrated in Figure 1, there is one major node called MCell (Master Cell, in accordance with 3GPP LTE terminology), which here is typically a microwave base station. However, functionally, the MCell can be any network entity that performs centralized handover and scheduling decisions. The UE may receive data from a number of cells, either mmWave or microwave, and we call each such cell an SCell (Secondary Cell). In order to

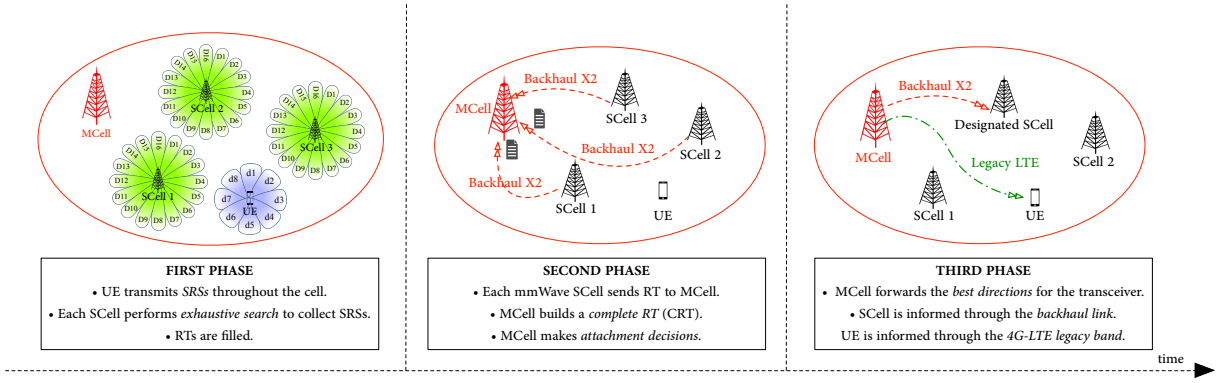

Figure 1: Slot scheme for the proposed MC procedure. After the first phase, each mmWave SCell builds a RT which is used to track the propagation conditions of its surrounding channels. Green and red dashed lines refer to the control messages exchanged via the legacy communication link and the backhaul X2 connection, respectively. In this figure, we assume that the MCell is identified as the macrowave base station. In this example, $N_{\mathrm{BS}} = 16$ (so the BS scans through $D_1, \ldots, D_{16}$ sectors), and $N_{\mathrm{UE}} = 8$ (so the UE sends the SRSs through $d_1, \ldots, d_8$ sectors).

communicate and exchange control information, the SCells and the MCell are inter-connected via traditional backhaul X2 interface connections, while each user can be reached by its serving MCell through the legacy 4G-LTE band.

MmWave SCells and UE will likely utilize directional phase arrays for transmission. In this work, we will assume that nodes select one of a finite number of directions, and we let N_{BS} and N_{UE} be the number of directions at each BS and UE, respectively. Thus, between any cell and the UE there are a total of $N_{\mathrm{BS}} \times N_{\mathrm{UE}}$ direction pairs. The key challenge in implementing multi-cell connectivity is that the network must, in essence, monitor the signal strength on each of the direction pairs for each of the possible links. This is done by each SCell building a report table (RT), based on the channel quality of each receiving direction, per each user, that can be used by the central entity to: (i) help the UE identify the mmWave BS with the best instantaneous propagation conditions[1], (ii) trace and estimate, over time, the channel quality conditions.

The system can be more precisely described as follows: Suppose that, in the considered area, M SCells are deployed under the control of one MCell. Our proposed method performs this monitoring through the three main phases.

[1]This is used in the initial access phase to select the BS to associate to, or in *connected mode*, to trigger a handover.

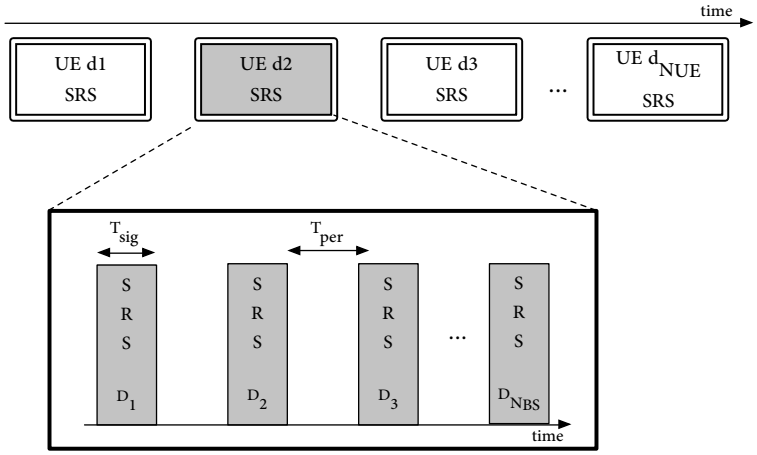

Figure 2: Slot scheme for the first phase of the proposed MC procedure. N_{BS} and N_{UE} are the number of directions at each BS and UE, respectively.

A. First phase: Uplink measurements

In the MC procedure's first phase, whose slot scheme is reported in Figure 2, each SCell fills its RT. The UE directionally broadcasts uplink sounding reference signals in dedicated slots, steering through directions $d_1, \ldots, d_{N_{\mathrm{UE}}}$, one at a time, to cover the whole angular space. The SRSs are scrambled by locally unique identifiers (e.g., C-RNTI) that are known to the SCells. We are therefore proposing an UL measurement reporting system where, unlike in traditional mechanisms, the reference signals are broadcast by each UE rather than by the base stations. The advantages of this design choice will be explained in the next sections of this work.

Each SCell performs an exhaustive search, scanning through directions $D_1, \ldots, D_{N_{\mathrm{BS}}}$,[2] in order to fill each row of the report table. For example, the i^{th} row of the RT refers to the user steering direction d_i and the quantity

$$\mathrm{SINR}_{i,j} = \max_{k=D_1,\ldots,D_{N_{\mathrm{BS}}}} \mathrm{SINR}_{i,j}(k) \tag{1}$$

represents the highest perceived SINR between the UE, transmitting through direction d_i, and SCell_j, maximized over all its possible receiving directions. The value

$$\mathrm{D}_{i,j} = D(\mathrm{SINR}_{i,j}) = D\Big(\max_{k=D_1,\ldots,D_{N_{\mathrm{BS}}}} \mathrm{SINR}_{i,j}(k)\Big) \tag{2}$$

[2]In the case of digital beamforming, the receiver would detect the signal strength from all directions in a single slot.

is the angular direction through which such $\text{SINR}_{i,j}$ was received by SCell_j.

Each mmWave SCell keeps a record of previous RTs and updates, at each scan, the variance $\text{var}_{i,j}$ of the maximum SINR, $\text{SINR}_{i,j}$. When, at scan t, SCell_j computes a new SINR value $\text{SINR}_{i,j}^{(t)}$, according to (1), the variance is updated as:

$$\begin{aligned} \text{var}_{i,j}^{(t)} &= \text{var}\left(\text{SINR}_{i,j}^{(1)}, \ldots, \text{SINR}_{i,j}^{(t)}\right) \\ &= \frac{\sum_{h=1}^{t}\left(\text{SINR}_{i,j}^{(h)}\right)^2}{t} - \left(\frac{\sum_{h=1}^{t}\text{SINR}_{i,j}^{(h)}}{t}\right)^2 \end{aligned} \tag{3}$$

using the SINR values of the previously saved report tables.

If the base station has finite memory and can keep a record of just U previous RT replicas, then the variance is updated as:

$$\begin{aligned} \text{var}_{i,j}^{(t)} &= \text{var}\left(\text{SINR}_{i,j}^{(t-U)}, \ldots, \text{SINR}_{i,j}^{(t)}\right) \\ &= \frac{\sum_{h=t-U}^{t}\left(\text{SINR}_{i,j}^{(h)}\right)^2}{U} - \left(\frac{\sum_{h=t-U}^{U}\text{SINR}_{i,j}^{(h)}}{U}\right)^2 \end{aligned} \tag{4}$$

The uplink SRS signals could also be monitored by cells that are not currently SCells to see if they should be added.

B. Second Phase: Network decision

Once the RT of each SCell has been filled, each mmWave cell sends this information, through the backhaul link, to the supervising microwave MCell which, in turn, builds a complete report table (CRT), as depicted in Table I. The macro cell has indeed a complete overview of the surrounding channel conditions and gains a comprehensive vision over the whole cellular system it oversees. When accessing the CRT, the MCell eventually makes a network decision by selecting the best mmWave BS candidate for the considered user, based on different metrics. For example, the MCell could select the maximum SINR (with some hysteresis) or the maximum rate (when knowing the current load of each cell), in order to have the best channel propagation conditions. So, as an example, according to the maximum SINR attachment policy:

$$(\text{CRT row}, \text{CRT col}) = (d_{\text{UE}}, n_{\text{ID}}) = \max_{\substack{i=d_1,\ldots,d_{N_{\text{UE}}} \\ j=1,\ldots,M}} \text{SINR}_{i,j}, \tag{5}$$

UE direction	**SCell**$_1$	**SCell**$_2$	**...**	**SCell**$_M$
1	$\text{SINR}_{1,1}$ $D_{1,1}$ $\text{var}_{1,1}$	$\text{SINR}_{1,2}$ $D_{1,2}$ $\text{var}_{1,2}$	...	$\text{SINR}_{1,M}$ $D_{1,M}$ $\text{var}_{1,M}$
2	$\text{SINR}_{2,1}$ $D_{2,1}$ $\text{var}_{2,1}$	$\text{SINR}_{2,2}$ $D_{2,2}$ $\text{var}_{2,1}$	...	$\text{SINR}_{2,M}$ $D_{2,M}$ $\text{var}_{2,M}$
...	...	...	...	...
N_{UE}	$\text{SINR}_{N_{\text{UE}},1}$ $D_{N_{\text{UE}},1}$ $\text{var}_{N_{\text{UE}},1}$	$\text{SINR}_{N_{\text{UE}},2}$ $D_{N_{\text{UE}},2}$ $\text{var}_{N_{\text{UE}},2}$	...	$\text{SINR}_{N_{\text{UE}},N_{\text{UE}}}$ $D_{N_{\text{UE}},N_{\text{UE}}}$ $\text{var}_{N_{\text{UE}},N_{\text{UE}}}$

Table I: An example of the complete report table that the MCell builds, after having received the partial RTs from the M surrounding mmWave SCells in the considered area. We suppose that the UE can send the sounding signals through N_{UE} angular directions.

where d_{UE} is the direction the UE should set to obtain the maximum SINR and reach the mmWave SCell with ID n_{ID}. Such maximum SINR is associated, in the CRT's entry, to the SCell direction D_{SCell}, which should therefore be selected by the mmWave BS to reach the UE with the best performance.

C. Third Phase: Path switch and scheduling command

If the serving cell needs to be switched, or a secondary cell needs to be added or dropped, the MCell needs to inform both the UE and the cell. Since the UE may not be listening in the direction of the target SCell, the UE may not be able to hear a command from that cell. Moreover, since path switches and cell additions in the mmWave regime are commonly due to link failures, the control link to the serving mmWave cell may not be available either. To handle these circumstances, we propose that the path switch and scheduling commands be communicated over the legacy 4G cell.

Therefore, the MCell notifies the designated mmWave SCell (with ID n_{ID}), via the high capacity backhaul, about the UE's desire to attach to it. It also embeds the best direction d_{SCell} that should be set to reach that user. Moreover, supposing that the UE has already set up a link to a macro cell base station, on a legacy LTE connection, the MCell sends to the UE, through an omnidirectional control signal at microwaves, the best user direction d_{UE} to select, to reach

such candidate SCell. By this time, the best SCell-UE beam pair has been determined, therefore the transceiver can directionally communicate in the mmWave band.

We recall that the attachment decision is neither performed by the user nor by the designated mmWave SCells, but rather by the supervising MCell, which is the only entity having a clear and complete periodic overview of the channel propagation conditions. This guarantees much more reliability (since the microwave cell is almost transparent to blockage absorption) and fairness (since the attachment decision can be periodically made by knowing the propagation conditions of the whole cellular network) in the communication system.

IV. Control Applications for MC Procedure

The proposed UL-based framework can be used to address some of the most important 5G control plane challenges that arise when dealing with mmWave frequency bands. In this section, we list some of the functions that are suitable to be implemented with our MC procedure.

A. Handover and Beam Tracking

Handover is performed when the UE moves from the coverage of one cell to the coverage of another cell [16]. Beam tracking refers to the need for a user to periodically adapt its steering direction, to realign with its serving BS, if it has moved or the channel propagation conditions have changed over time. Frequent handover, even for fixed UEs, is a potential drawback of mmWave systems due to their vulnerability to random obstacles, which is not the case in LTE. Dense deployments of short range BSs, as foreseen in mmWave cellular networks, may exacerbate frequent handovers between adjacent BSs. Loss of beamforming information due to channel change is another reason for handover and reassociation [10]. There are only a few papers on handover in mmWave 5G cellular [17]–[20], since research in this field is just in its infancy.

Our proposed procedure exploits the centralized-MCell control over the network, which can be used to periodically determine the UE's optimal mmWave SCell (and direction) to associate with, or its new direction through which it should steer the beam, when the user is in *connected-mode*, i.e., it is already synchronized with both the macro and the mmWave cells. The key input information for the handover/beam tracking decision includes (i) instantaneous channel quality, (ii) channel variance, and (iii) cell occupancy.

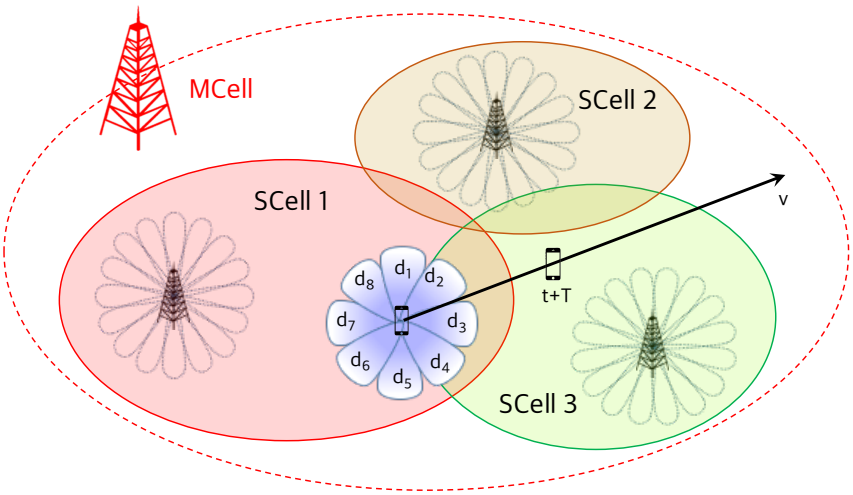

Figure 3: Handover in mmWave cellular networks. UE moves at constant velocity v. Solid (and dashed) ellipses show mmWave (and microwave) coverage boundaries (idealized for ease of discussion).

Assume that a new RT is collected at the SCell side and forwarded to the MCell, after the proposed three-phase MC procedure has been completed. By accessing the table, if the UE's optimal mmWave cell is different from the current one, then a handover should be triggered, to maximize the user SINR or rate[3]. Moreover, if a new steering direction is able to provide a higher rate to the user, a beam switch can be prompted, to realign with the BS and guarantee better communication performance.

As an example, we refer to Figure 3. Suppose that, at time t, the user is attached to SCell 1 and keeps moving in a fixed direction at constant speed v. When, at time $t + T$, the MCell collects a new CRT, it can decide whether or not to make the user perform a handover to another mmWave cell (i.e., SCell 3, if this could increase the user's QoS), to just switch the beam or even not to take any action at all.

With respect to the existing algorithms, the use of both the microwave and the mmWave control planes is a key functionality for such a technique. In fact, in the third phase, the handover/beam switch decision is forwarded to the UE through the MCell, whose microwave link is much more

[3]In order to reduce the handover frequency, more sophisticated decision criteria could be investigated, rather than triggering a handover every time a more suitable SCell is identified (i.e., the reassociation might be performed only if the SINR increases above a predefined threshold, with respect to the previous time instant). A more detailed discussion of the different handover paradigms is beyond the scope of this paper.

robust and less volatile than its mmWave counterpart, thereby removing a possible point of failure in the control signaling path. Since each SCell periodically forwards the RT, the MCell has a complete overview of the cell dynamics and propagation conditions and can accordingly make network decisions, to maximize the overall performance of the cell it oversees.

Moreover, the attachment policy can also take care of the capacity of each mmWave base station, unlike in the traditional procedures in which the users are not aware of the surrounding cells' current state. Thus, the UE may choose to connect to the SCell providing either the maximum SINR or the maximum rate, depending on what is considered more convenient.

We finally remark that if previous versions of the report table are kept as a record, the MCell can also use the SCells variance in selecting the mmWave cell a user should attach to, after a handover is triggered. If a selected SCell shows a large variance (which reflects high channel instability), the user might need to handover again in the very near future. Therefore, it could be better to trigger a handover only to an SCell which grants both good SINR (or rate) and sufficient channel stability, leading to a more continuous and longer-term association with such designated cell. We address this analysis as part of our future work.

B. Multi-Cell Initial Access

The procedure described in Sections III and IV-A referred to a UE that is already connected to the network. However, we show that the uplink based control may also be leveraged for fast initial access from idle mode. Initial access (IA) is the procedure by which a mobile UE establishes an initial physical link connection with a cell, a necessary step to access the network. In current LTE systems, IA is performed on omnidirectional channels [16]. However, in mmWave cellular systems, transmissions will need to be directional to overcome the increased isotropic pathloss experienced at higher frequencies. IA must thus provide a mechanism by which the BS and the UE can determine suitable initial directions of transmission.

MmWave IA procedures have been recently analyzed in [7], [21]–[23]. Different design options have been compared in [24] and [25], to evaluate coverage and access delay. We refer to [25] for a more detailed survey of recent IA works. All of these methods are based on the current LTE design where each cell broadcasts synchronization signals and the UE scans the directional space to detect those signals and find the optimal base station to potentially connect to. We will call these "downlink" based designs, since the transmissions come from the BSs to the UEs. A

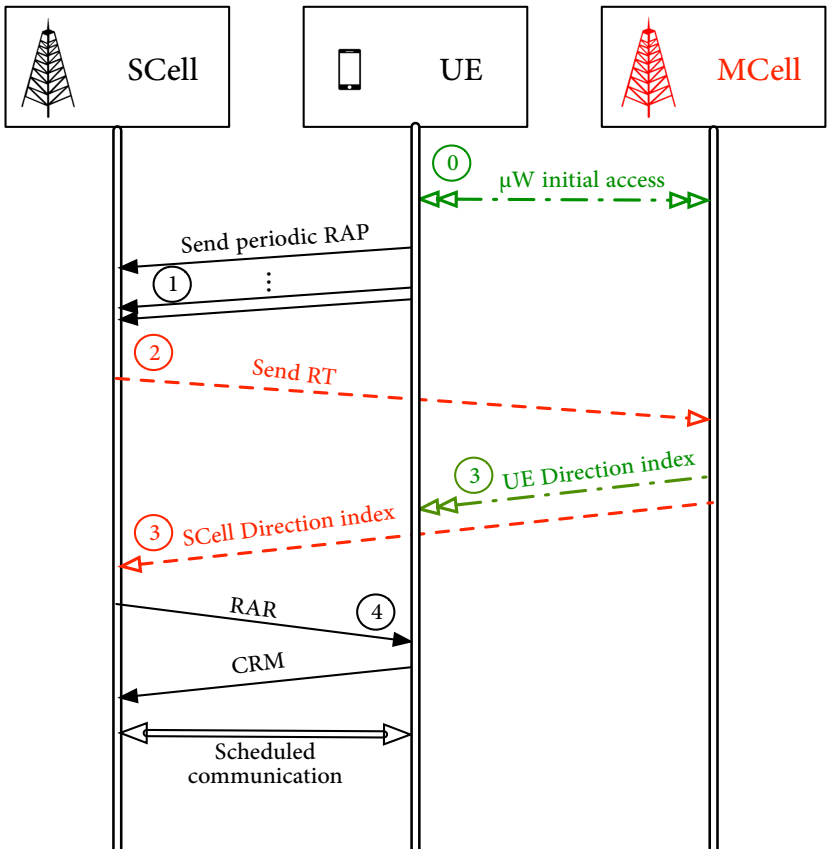

Figure 4: Proposed multicell initial access procedure. Both the macro MCell and the SCell base stations play a role in this cell selection technique, where the presented MC algorithm is also used. Red and green dashed lines refer to the control messages exchanged via the bachaul X2 and the legacy communication links, respectively.

key result of these findings is that the dominant delay in downlink-based IA arises in this initial sychronization phase.

In this work, we propose an alternate "uplink" scheme, mainly based on the proposed MC procedure described in Section III, as shown in Figure 4.

0) A UE first searches for synchronization signals from conventional 4G cells. This detection is fast since it can be performed omnidirectionally and there is no directional scanning. Under the assumption that the 5G mmWave cells are roughly time synchronized to the 4G cell, and the round trip propagation times are not large, an uplink transmission from the UE will be roughly time aligned at any closeby mmWave cell. For example, if the cell radius is 150 m (a typical mmWave cell), the round trip delay is only 3 μs.

1) A UE desiring initial access broadcasts a random access preamble (RAP) scanning different angular directions, while the mmWave cells scan for the presence of those messages. As in the MC procedure's first phase, multiple RTs are collected at the SCell sides. Each of these RAPs will arrive roughly time-aligned in the random access slots of all potential neighboring mmWave cells.
2) Each SCell forwards its RT to the MCell via the X2 backhaul link. In analogy with the MC's second phase, the MCell performs the best attachment decision, based on the received RT, together with selecting the optimal directions for the transceiver to communicate.
3) The MCell forwards to the designated SCell (via the usual high capacity backhaul) and to the user (via the legacy LTE band though an omnidirecional control message) the respective sectors through which they should steer the beam to communicate.
4) At this point, the best SCell-UE beam pair has been determined, therefore both the user and the SCell can steer through their optimal directional sectors, obtaining the full beamorming gain. So, the SCell transmits a random access response (RAR) to the UE, containing some initial timing and power correction information. After receiving the RAR, the UE sends a connection request message (CRM) on the resources scheduled in the uplink grant in the RAR. All subsequent communication can occur on scheduled channels. In 3GPP LTE, the immediate subsequent messages would be used for connection set up and contention resolution [21].

One of the most important features of the presented IA procedure is that the attachment decision is made by the MCell, which oversees the whole network and collects channel reports from all surrounding mmWave cells. Therefore, unlike in the traditional attachment policies that could just rely on the instantaneous perceived signal strengths of the surrounding base stations, the association can be possibly performed by selecting the user's most profitable cell to guarantee enough fairness and reliability for the whole cellular network, as shown in Section VI-B.

To compare uplink and downlink based IA, first suppose that the BS and the UE can transmit and receive in only one direction at a time. In this case, in either DL or UL-based synchronization, the BS and the UE must search all $N_{\mathrm{BS}}N_{\mathrm{UE}}$ direction pairs and hence both UL and DL-based IA will take roughly the same time. To reduce the search time, the receiver (the BS in the UL case and the UE in the DL case) must be able to search in multiple directions simultaneously, via either hybrid or digital beamforming. Suppose that the receiver can look in L directions.

Then, the scan time would be reduced by a factor of L to $N_{\mathrm{BS}}N_{\mathrm{UE}}/L$. In particular, if the BS could perform fully digital reception and hence look in all $L = N_{\mathrm{BS}}$ directions at the same time, the UL-based IA would require only N_{UE} scans. Similarly, if the UE could perform fully digital reception, the DL procedure would require N_{BS} scans.

The reason the uplink-based IA may be preferable is that hybrid or fully digital receivers are more costly in terms of power consumption, and hence are more likely to be implemented in a BS rather than in a UE. In this case, the delay gains can be significant. We will evaluate these gains precisely in Section VI-B.

C. Blockage Reaction

One of the key challenges for cellular systems in mmWave bands is the rapid channel dynamics. Differently from current LTE systems, mmWave signals are completely blocked by many common building materials such as brick and mortar. As a result, the movement of obstacles and reflectors, or even changes in the orientation of a handset relative to a body or hand, can cause the channel to rapidly appear or disappear [26]. When a radio link failure occurs, the link that has been established between user and base station is obstructed, with a consequent SINR degradation and throughput collapse. The UE should immediately react by adapting its beam pair or, as a last resort, by triggering a handover [8].

Most literature refers to challenges that have been recently analyzed in the 60 GHz IEEE 802.11ad WLAN and WPAN scenarios. In [27], for example, a detailed investigation of the effect of people movement on the temporal fading envelope is performed. Some related works present different solutions to address the blockage issue described above, such as [28]–[30].

Our MC procedure can be implemented to partially solve the failure and blockage problems, making use of the much more reliable and stable legacy LTE connection that the user can exploit. We use Figure 5 as an example.

Assume that, at time t, the user moving at constant speed v is connected to a specific mmWave BS, through direction d_{opt}, granting the maximum rate. We assume that, at time $t+x$ and before a new RT is generated, a blockage occurs, obstructing the best path that was linking the UE and the BS. If no practical actions are taken, the user has to wait for a new RT (collected at time $t+T$) before a new optimal beam pair, able to circumvent the obstruction, is determined. Indeed, during $T-x$ seconds, the user's rate is zero, due to the link breakdown and the consequent SINR

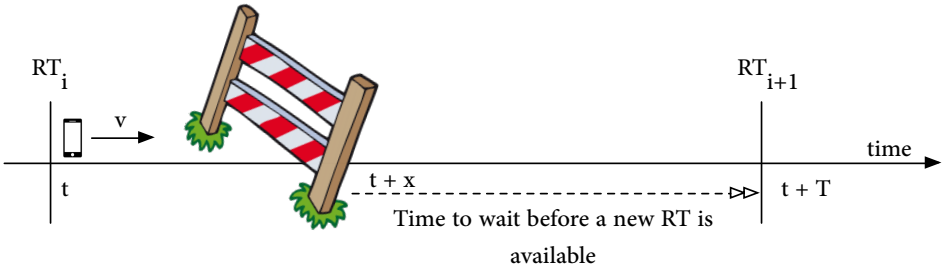

Figure 5: MC procedure for RLF and blockage reaction. At time t and $t+T$ the UE collects a RT. At time $t+x$ a blockage event occurs and the user, moving at constant velocity v, loses the connection with its current serving mmWave BS. The UE and the BS can suddenly react to the channel failure by exploiting previously saved report tables.

slump. One practical solution is to immediately react to the blockage by exploiting previously saved instances of the RT. As soon as a blockage is detected, the UE and the designated BS can autonomously access their most recent RT (or set of previous tables) and find the second best direction $d_{\text{subopt}} \neq d_{\text{opt}}$ to communicate. Such beam pair will be a suboptimal solution (since the optimal path is blocked), but at least the user can achieve a higher average throughput than it would have achieved if no action were taken.

Having a second available link, when the primary path is obstructed, obviously adds a lot of diversity and robustness to the communication. According to our MC algorithm, the RT is used to find such suboptimal alternate link, after a RLF occurs, as a sort of *backup procedure* before the user fully recovers the optimal SCell-UE link, upon collecting a new and updated RT.

In Section VI we show the advantages, in terms of throughput, of establishing a backup direction between user and BS, after a blockage occurs, rather than just waiting for a new RT to be received.

V. Simulation Parameters Description

The parameters used to run our simulations are based on realistic system design considerations and are summarized in Table II.

A. MmWave Channel Model

The channel model we have implemented is based on recent real-world measurements at 28 GHz in New York City, to provide a realistic assessment of mmWave micro and picocellular

Parameter	Value	Description
W_{tot}	1 GHz	Total system bandwidth
DL P_{TX}	30 dBm	Downlink transmission power
NF	5 dB	Noise figure
f_{c}	28 GHz	Carrier frequency
τ	-5 dB	Minimum SINR threshold
SCell antenna	8×8	BS UPA MIMO array size
UE antenna	4×4	UE UPA MIMO array size
N_{BS}	16	SCells scanning directions
N_{UE}	8	UE scanning directions
A	0.5 km^2	Area of the simulation
T_{sig}	10 μs	SRS duration
ϕ_{ov}	5%	Overhead
T_{per}	200 μs	Period between SRS transmissions
T_B	varied	Blockage duration
T_H	varied	Update interval of **H** matrix
T_{RT}	varied	Time between two consecutive RTs
D	varied	mmWave BS density (BS/km^2)
N	10 per BS	Number of users

Table II: Simulation parameters.

networks in a dense urban deployment. The link budget for the mmWave propagation channel is defined as:

$$P_{RX} = P_{TX} + G_{BF} - PL - \xi \tag{6}$$

where P_{RX} is the total received power expressed in dBm, P_{TX} is the transmit power, G_{BF} is the gain obtained using BF techniques, PL represents the pathloss in dB and $\xi \sim N(0, \sigma^2)$ is the shadowing in dB, whose parameter σ^2 comes from the measurements in [2].

Based on the real-environment measurements of [2], the pathloss can be modeled through three different states: Line-of-Sight (LoS), Non-Line-Of-Sight (NLoS) and outage. Based on the distance d between the transmitter and the receiver, the probability to be in one of the states

(P_{LoS}, P_{NLoS}, P_{out}) is computed by:

$$\begin{aligned} P_{\text{out}}(d) &= \max(0, 1 - e^{-a_{\text{out}}d + b_{\text{out}}}) \\ P_{\text{LoS}}(d) &= (1 - P_{\text{out}}(d))e^{-a_{\text{LoS}}d} \\ P_{\text{NLoS}}(d) &= 1 - P_{\text{out}}(d) - P_{\text{LoS}}(d) \end{aligned} \tag{7}$$

where parameters $a_{\text{out}} = 0.0334$ m^{-1}, $b_{\text{out}} = 5.2$ and $a_{\text{LoS}} = 0.0149$ m^{-1} have been obtained in [2] for a carrier frequency of 28 GHz. The pathloss is finally obtained by:

$$PL(d)[dB] = \alpha + \beta 10 \log_{10}(d) \tag{8}$$

where d is the distance between receiver and transmitter, and the value of the parameters α and β are given in [2].

To generate random realizations of the large-scale parameters, the mmWave channel is defined as a combination of a random number $K \sim \max\{\text{Poisson}(\lambda), 1\}$ of path clusters, for which the parameter λ can be found in [2], each corresponding to a macro-level scattering path. Each cluster is further composed of several subpaths $L_k \sim U[1, 10]$, according to [31].

The time-varying channel matrix is described as follows:

$$\mathbf{H}(t, f) = \frac{1}{\sqrt{L}} \sum_{k=1}^{K} \sum_{l=1}^{L_k} g_{kl}(t, f) \mathbf{u}_{rx}(\theta_{kl}^{rx}, \phi_{kl}^{rx}) \mathbf{u}_{tx}^{*}(\theta_{kl}^{tx}, \phi_{kl}^{tx}) \tag{9}$$

where $g_{kl}(t, f)$ refers to the small-scale fading over time and frequency on the l^{th} subpath of the k^{th} cluster and $\mathbf{u}_{rx}(\cdot)$, $\mathbf{u}_{tx}(\cdot)$ are the spatial signatures for the receiver and transmitter antenna arrays and are functions of the central azimuth (horizontal) and elevation (vertical) Angle of Arrival (AoA) and Angle of Departure (AoD), respectively θ_{kl}^{rx}, ϕ_{kl}^{rx}, θ_{kl}^{tx}, ϕ_{kl}^{tx} [4].

The small-scale fading in Equation (9) describes the rapid fluctuations of the amplitude of a radio signal over a short period of time or travel distance. It is generated based on the number of clusters, the number of subpaths in each cluster, the Doppler shift, the power spread, and the delay spread, as:

$$g_{kl}(t, f) = \sqrt{P_{lk}} e^{2\pi i f_d \cos(\omega_{kl}) t - 2\pi i \tau_{kl} f}, \tag{10}$$

where:

[4]Such angles can be generated as wrapped Gaussian around the cluster central angles with standard deviation given by the rms angular spread for the cluster given in [2].

- P_{lk} is the power spread of subpath l in cluster k, as defined in [2];
- f_d is the maximum Doppler shift and is related to the user speed v and to the carrier frequency f as $f_d = fv/c$, where c is the speed of light;
- ω_{kl} is the angle of arrival of subpath l in cluster k with respect to the direction of motion;
- τ_{kl} gives the delay spread of subpath l in cluster k;
- f is the carrier frequency.

Due to the high pathloss experienced at mmWaves, multiple antenna elements with beamforming are essential to provide an acceptable communication range. The BF gain parameter in (6) from transmitter i to receiver j is thus given by:

$$G_{BF}(t,f)_{ij} = |\mathbf{w}^*_{rx_{ij}}\mathbf{H}(t,f)_{ij}\mathbf{w}_{tx_{ij}}|^2 \tag{11}$$

where $\mathbf{H}(t,f)_{ij}$ is the channel matrix of the ij^{th} link, $\mathbf{w}_{tx_{ij}} \in \mathbb{C}^{n_{\mathbb{T}x}}$ is the BF vector of transmitter i when transmitting to receiver j, and $\mathbf{w}_{rx_{ij}} \in \mathbb{C}^{n_{\mathbb{R}x}}$ is the BF vector of receiver j when receiving from transmitter i. Both vectors are complex, with length equal to the number of antenna elements in the array, and are chosen according to the specific direction that links BS and UE.

The channel quality is measured in terms of SINR. By referring to the mmWave statistical channel described above, the SINR between BS j and a test UE can be computed in the following way:

$$\text{SINR}_{j,\text{UE}} = \frac{\frac{P_{\text{TX}}}{PL_{j,\text{UE}}}G_{j,\text{UE}}}{\sum_{k\neq j}\frac{P_{\text{TX}}}{PL_{k,\text{UE}}}G_{k,\text{UE}} + W_{\text{tot}} \times N_0} \tag{12}$$

where $G_{i,\text{UE}}$ and $PL_{i,\text{UE}}$ are the BF gain and the pathloss obtained between SCell$_i$ and the UE, respectively, and $W_{\text{tot}} \times N_0$ is the thermal noise. In (12), it is assumed that the UE is interfered by other transmitters. However, to some extent, all cells have their own control plane which removes any inter-cell interference. According to the different instantaneous SCell and UE pointing directions, different beamforming gains are obtained and potentially different SINR values are perceived and collected.

Finally, the rate (R) is approximated using the Shannon capacity:

$$R_{j,\text{UE}} = \frac{W_{\text{tot}}}{N}\log_2(1 + \text{SINR}_{\text{j,UE}}) \tag{13}$$

where N is the number of users that are currently being served by SCell$_j$.

B. Simulated Scenarios

Our results are derived through a Monte Carlo approach, where multiple independent simulations are repeated, to get different statistical quantities of interest. In each experiment: (i) we deploy multiple mmWave base stations and multiple UEs, according to a Poisson Point Process (PPP), as done in [32], with an average density of 10 users per cell; (ii) we perform the multi-connectivity algorithm by establishing a mmWave link between each SCell-UE pair and collecting the SINR values at each SCell, according to Equation (12), when the transceiver performs the sequential scan; and (iii) we select the most profitable mmWave cell the user should attach to, according to either a maximum SINR or maximum rate policy.

Referring explicitly to the MC procedures, we consider an SINR threshold $\tau = -5$ dB, assuming that, if $\text{SINR}_{i,j}(k) < \tau$, no control signals are collected when the UE transmits through direction i and the BS j is steering through direction k. Reducing τ allows the user to be potentially found by more suitable mmWave cells, at the cost of designing more complex (and expensive) receiving schemes, able to detect the intended signal in more noisy channels. A set of two dimensional antenna arrays is used at both the mmWave SCells and the UE. BSs are equipped with a Uniform Planar Array (UPA) of 8×8 elements, which allow them to steer beams in $N_{\text{BS}} = 16$ directions; the user exploits an array of 4×4 antennas, steering beams through $N_{\text{UE}} = 8$ angular directions. The spacing of the elements is set to $\lambda/2$, where λ is the wavelength.

According to [21], [24] and Figure 2, we assume that the SRSs are transmitted periodically once every $T_{\text{per}} = 200\ \mu s$, for a duration of $T_{\text{sig}} = 10\ \mu s$ (which is deemed sufficient to allow proper channel estimation at the receiver), to maintain a constant overhead $\phi_{\text{ov}} = T_{\text{sig}}/T_{\text{per}} = 5\%$.

C. Mobility Model

The test user moves in a fixed direction, at a constant speed v. We set $v = 1.3$ m/s, to simulate a walking user, and $v = 20$ m/s for a user moving by car. One of the key challenges for cellular systems in the mmWave bands is the rapid channel dynamics. When moving, the user experiences a strong Doppler shift whose effect increases with speed. Therefore, we need to periodically update both the small and the large scale fading parameters of the $\mathbf{H}$ matrix in Equation (9), to emulate short fluctuations and sudden changes of the perceived channel, respectively.

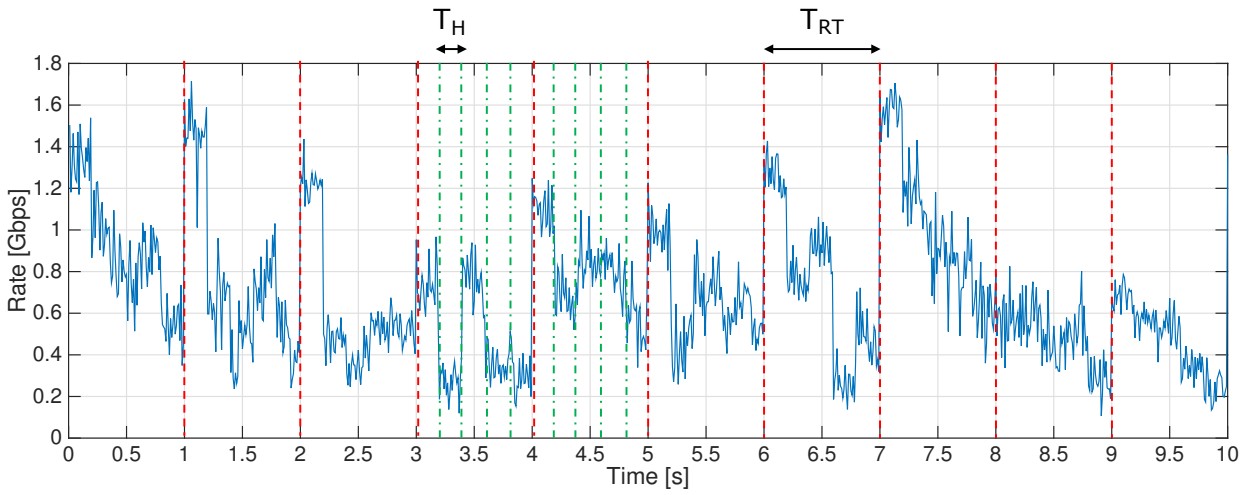

Figure 6: Example of time-varying rate experienced by a user moving at constant speed $v = 20$ m/s, in a mmWave scenario where $D = 70$ BS/km^2 are deployed. The RTs are generated every $T_{\mathrm{RT}} = 1$ s (red dashed lines), the small scale fading parameters of the channel matrix $\mathbf{H}$ vary every 1 ms, the large scale fading parameters of the channel matrix $\mathbf{H}$ vary every $T_H = 200$ ms (green dotted lines).

The Doppler shift and the spatial signatures are updated at every time slot, according to the user speed and its position (AoA, AoD). The distance-based pathloss is also updated, but we maintain the same pathloss state (LoS, NLoS or outage) recorded in the previous complete update of the $\mathbf{H}$ matrix. On the other hand, every T_H seconds, the $\mathbf{H}$ matrix is completely updated, to capture the effects of the long term fading. Therefore, we update all the statistical parameters of the channel, like the number of spatial clusters and subpaths, the fractions of power, the angular beamspreads and the pathloss conditions, for all the mmWave links between each UE and each SCell. We recall that this may cause the user to switch from a certain pathloss state to another one (e.g., from LoS to NLoS, to simulate the presence of an obstacle between transmitter and receiver), with a consequent sudden drop of the channel quality by many dBs.

The beamforming vectors are not adapted when the $\mathbf{H}$ matrix is updated. We need to wait for a RT (received every T_{RT} seconds) to detect the (possibly changed) channel propagation conditions and properly react by adapting the directions through which the UE and the designated SCell steer the beams. Frequent RTs (small T_{RT}) and flat channels (large T_H) result in a good monitoring of the user's motion and good average channel gains. In Section VI-A we show how a variation of T_{RT} and T_H affects in the communication quality.

We plot in Figure 6 an example of rate and cell association trends, along with an intuitive representation of the effect of updating the report table every T_{RT} seconds and the channel matrix every T_H seconds. For example, it can be seen that, at time $t = 1^-$, the user's rate has been strongly degraded, since the user has moved without updating its beam towards its BS and thus has misaligned. However, at time $t = 1^+$, a new RT has been received and the transceiver is finally able to update its beam pair (by performing a beam switch) or the user can handover (by choosing a serving BS providing better communication performance), thus recovering the maximum transmission rate. We notice that wide rate collapses mainly refer to pathloss state changes (i.e., from LoS to NLoS), caused by the update of the large scale fading parameters of the mmWave channel, while the rapid fluctuations of the rate are due to adaptation of the small scale fading parameters of $\mathbf{H}$ (and mainly to the Doppler effect experienced by the moving user).

VI. Results

In this section, we present some results that have been derived for each control applications introduced in Section IV, to show that:

(i) periodical RTs can be used to trigger handovers or adapt the beam pair of the user and its serving mmWave BS over time, to grant good average throughputs and maintain acceptable communication performance;

(ii) UL-based multi-cell IA can offer significantly reduced latency in the presence of digital beamforming at the BS and a rate-based attachment policy can provide more fairness to the whole cellular network;

(iii) having a second available link, rather than just waiting for a new RT to be received, when the primary path is obstructed, increases the average throughput for a user.

A. Results for Handover and Beam Tracking

The test user moves at a constant speed $v = 20$ m/s towards a specific direction. Due to its motion and to the variability of the mmWave channel over time, it needs to periodically trigger a handover or switch its transmitting beam, to recover a good communication quality. The large scale fading parameters of the channel are updated every T_H seconds, while the small scale fading parameters are constantly updated every time slot. When building a new CRT every T_{RT} seconds, the MCell can select, by looking at the best saved entry, the new serving SCell for

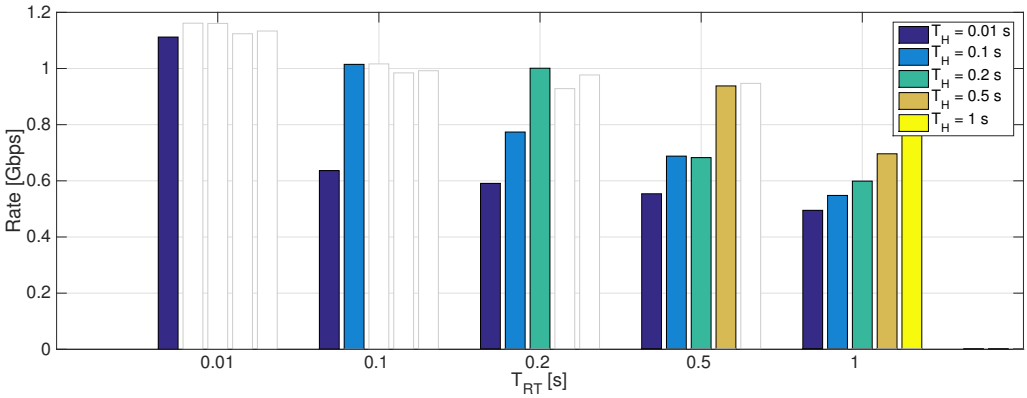

(a) Average rate vs. RT periodicity T_{RT}, for different values of T_H. The BS density is kept constant to 70 BS/km^2. White bars are referred to not remarkable cases, since $T < T_H$.

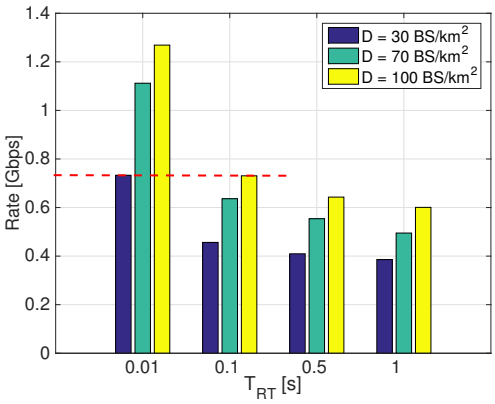

(b) Average rate vs. RT periodicity T_{RT}, for different BS densities. The large scale fading parameters of the channel are updated every $T_H = 10$ ms.

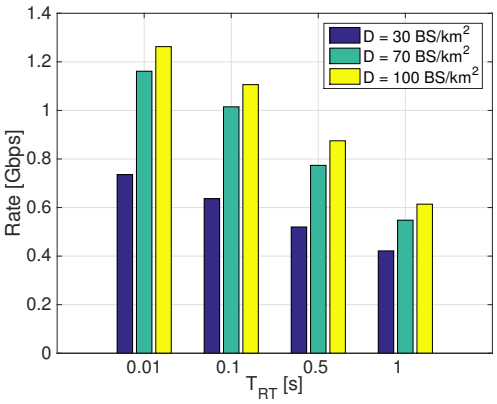

(c) Average rate vs. RT periodicity T, for different BS densities. The large scale fading parameters of the channel are updated every $T_H = 100$ ms.

Figure 7: Results of the simulations for handover and beam tracking procedures. The user moves at a constant speed $v = 20$ m/s.

the UE, or just select the new beam pair the transceiver has to set, in order to maximize the communication throughput.

We just consider the case $T \geq T_H$, otherwise the rate would be constant for all values of T_H (since the beam pair would be updated before the channel even changes its large scale fading parameters).

According to Figure 7(a), when T_{RT} increases, the average rate decreases, since the RTs are exchanged less frequently and the beam pair between the user and its serving SCell is

monitored less intensively. This means that, when the channel changes (due to a pathloss condition modification or to an adaptation of the propagation characteristics) or when the user misaligns with its SCell (due to its motion), the communication quality is not immediately recovered and the throughout is affected by portions of time where suboptimal network settings are chosen. We also observe that, when T_H increases, the average rate also increases since the channel varies less rapidly, so the rate can assume more stable values even if the SCell-UE beam pair is updated less frequently. In fact, a change in the **H** matrix's large scale fading parameters represents the strongest cause for the user's rate slump, but if we consider flat and stable channels, we can accept rarer report tables (and therefore trigger rarer handover and beam switch events) and still provide a sufficiently good communication quality.

According to Figures 7(b) and (c), when increasing the mmWave BS density D, the average rate also increases. In fact, the inter-cell distance is reduced and each UE generally finds a closer BS (showing better channel propagation conditions) to associate with, thus perceiving an increased SINR which reflects in an increase average rate, according to (13). Moreover, higher throughput values are collected when $T_H = 100$ ms (Figure 7(c)), since the channel changes less rapidly. Additionally, if we observe Figure 7(b), we note how a 0.75 Gbps rate (red dashed line), can be achieved either with a 30 BS/km^2 density and 0.01 second T_{RT}, or with a 100 BS/km^2 density and 0.1 second T_{RT}: The tradeoff oscillates between infrastructure cost and signaling overhead.

It is interesting to notice that the main advantage when increasing the cell density is observed from $D = 30$ BS/km^2 to $D = 70$ BS/km^2. In fact such rate gain reflects the transition from a user outage regime to a LoS/NLoS regime while, as we persistently keep on densifying the network, the deployment of more SCells leads to a considerable increase of the system complexity, while providing a limited increase of the rate.

B. Results for Multi-Cell Initial Access

Delay Analysis We start with the delay analysis of the multi-cell IA algorithm presented in Section IV-B. Following [7], [21], we suppose that in either the uplink or the downlink direction, the random access or synchronization signals are T_{sig} long and occur once ever T_{per} seconds. The size of T_{sig} is determined by the necessary link budget and we will assume that it is the same in both directions. The values in Table II are based on simulations in [7] that enable

BF Architecture		**DL-based** SCell transmits UE receives	**UL-based** SCell receives UE transmits
SCell Side	**UE Side**		
Analog	Analog	$N_{\mathrm{UE}}N_{\mathrm{BS}}$ (25.6 ms)	$N_{\mathrm{UE}}N_{\mathrm{BS}}$ (25.6 ms)
Analog	Digital	N_{BS} (3.2 ms)	$N_{\mathrm{UE}}N_{\mathrm{BS}}$ (25.6 ms)
Digital	Analog	$N_{\mathrm{UE}}N_{\mathrm{BS}}$ (25.6 ms)	N_{UE} (1.6 ms)
Digital	Digital	N_{BS} (3.2 ms)	N_{UE} (1.6 ms)

Table III: Number of synchronization signals (or RAPs) that the BS (or the UE) has to send (and corresponding time) to perform a DL (or UL) based procedure. A comparison among different BF architectures (analog and fully digital) is performed. We assume $T_{\mathrm{sig}} = 10\,\mu$s, $T_{\mathrm{per}} = 200\,\mu$s (to maintain an overhead $\phi_{\mathrm{ov}} = 5\%$), $N_{\mathrm{UE}} = 8$ and $N_{\mathrm{BS}} = 16$.

reliable detection with an overhead of $T_{\mathrm{sig}}/T_{\mathrm{per}}$ of 5%. Now, as discussed in Section IV-B, the scanning for either the synchronization signal in the downlink or the random access preamble in the uplink will require $N_{\mathrm{BS}}N_{\mathrm{UE}}/L$ scans, where L is the number of directions in which the receiver can look at any one time. Since there is one scanning opportunity every T_{per} seconds, the total delay is

$$\text{Delay} = \frac{N_{\mathrm{BS}}N_{\mathrm{UE}}T_{\mathrm{per}}}{L}.$$

The value of L depends on the beamforming capabilities. In the uplink-based design, $L = 1$ if the BS receiver has analog BF and $L = N_{\mathrm{BS}}$ if it has a fully digital transceiver. Similarly, in the downlink $L = 1$ if the UE receiver has analog BF and $L = N_{\mathrm{UE}}$ if it has a fully digital transceiver. Table III compares the resulting delays for UL- and DL-based designs depending on the digital BF capabilities of the UE and the BS. As discussed above, digital BF is much more likely at the BS than at the UE due to power requirements.

We see that, in this case, the UL design offers significantly reduced access delay, by making it possible to generate a new RT every at least 1.6 ms (when considering an overhead $\phi_{\mathrm{ov}} = 5\%$). However, according to the results in Section VI-A and in Figure 7(a), the user can experience quite good throughput values even when considering less frequent RT updates, if the channel is sufficiently flat and stable. Therefore we state that we can further reduce the overhead (to decrease the system complexity) and so design more sporadic channel updates, while guaranteeing sufficiently good network performance.

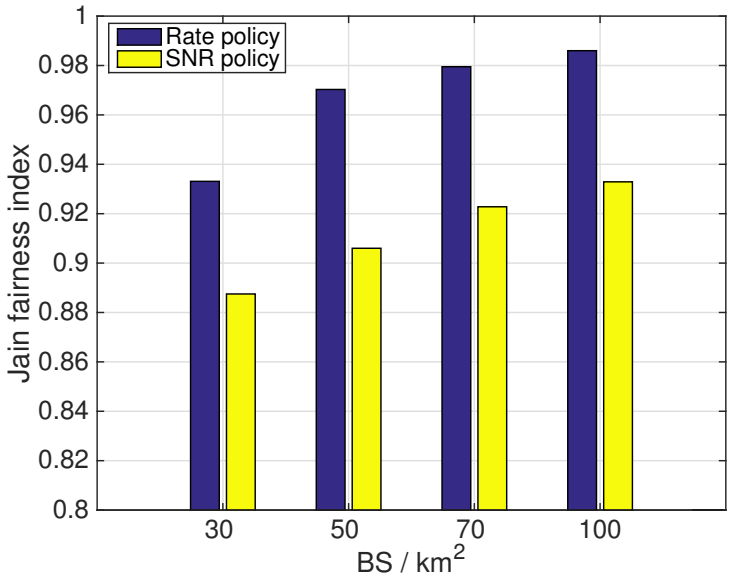

Figure 8: Jain's fairness index of the rate vs. mmWave BS density, for the multi-cell initial access procedure, when users within an area of radius $R_C = 70$ m attach to their best SCell according to a maximum rate or maximum SINR policy.

Load-Aware IA As pointed in Section IV-B, the use of the supervising 4G-LTE MCell when implementing the initial access procedure can provide the user two different attachment policies, unlike in the traditional schemes. The user may in fact connect to the SCell providing the highest SINR (max-SNR rule) or, knowing the current load of each BS, to the SCell providing the highest rate (max-rate rule).

In order to compare the average rate of users that perform initial access according to one of the two presented attachment policies, we use *Jain's fairness index*, which is used to determine whether users are receiving a fair share of the system resources and are thus experiencing a rate comparable to that of other users in the cellular system. This index is defined as:

$$J = \frac{\left(\sum_{i=1}^{N} x_i\right)^2}{N \sum_{i=1}^{N} x_i^2}, \tag{14}$$

and rates the fairness of a set of values where there are N users and x_i is the rate experienced by the i^{th} user. The result ranges from $1/N$ (worst case) to 1 (best case), and it is maximum when all users receive the same allocation.

In Figure 8, we plot Jain's fairness index for the rate experienced by users within an area of radius $R_C = 70$ meters, when attaching either according to the max-SINR rule (as in traditional

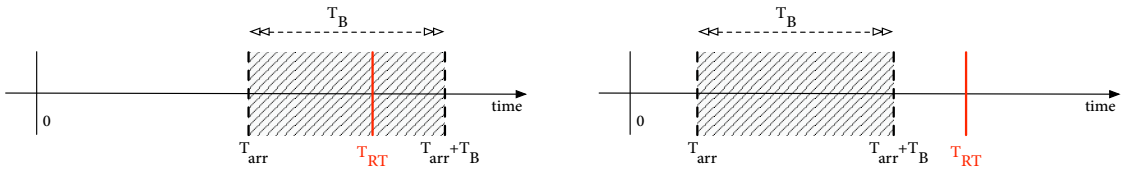

(a) Obstacle is still present, when the new RT is available.

(b) Obstacle is no longer present, when the new RT is available.

Figure 9: Blockage scenarios. The report tables are available every T_{RT} seconds, the obstacle duration is T_B seconds and is detected after T_{arr} seconds.

schemes) or the max-rate rule (by exploiting the MC procedure). As expected, this last attachment policy provides much higher fairness to the cellular system, since users try to connect to the SCell providing the maximum rate. Asymptotically, according to Equation (13), the mmWave cells will almost serve the same number of users N, and so a UE accessing the network at time t will likely find all the SCells in the same load conditions, providing comparable rates. On the other hand, by following a max-SINR attachment policy, users will tend to connect to the same BSs showing the instantaneous highest signal strengths (and thus overloading them), and avoiding instead cells that provide lower SINR values (but possibly higher rates, due to their low traffic loads). In this way, users might unfairly attach to BSs providing unbalanced throughput values, by increasing the rate variance of the system.

We finally notice that Jain's fairness index in Figure 8 increases as D increases. In fact, when densifying the network, the BSs ensure more similar propagation conditions to the users, which in turn perceive more balanced SINR (and rate) values.

C. Results for Blockage Reaction

According to the scenario described in Section IV-C, the optimal rate when no obstacles affect the network is R, while the suboptimal rate, when a suboptimal backup beam pair is selected, after the primary path is obstructed, is r[5].

[5]If no actions are taken to overcome the blockage, then $r = 0$ bps, meaning that the rate experienced by the user is zero, when an obstacle obstructs the primary path.

Assume that the RT periodicity is T_{RT} seconds and a blockage event is detected at time $T_{\mathrm{arr}} \sim \mathcal{U}(0, T_{\mathrm{RT}}) = T_{\mathrm{RT}}p$, with $p \in (0, 1)$, and lasts for T_B seconds. We aim at finding the *rate gain* (R_G), namely the ratio between the rate experienced when the MC procedure is used to establish a backup beam pair between the user and its serving SCell after a blockage is detected (R_{WB}), and the rate perceived when no actions are taken (R_{OB}). The analysis is distinguished between the following two cases.

Case 1: obstacle is still present, when the new RT is generated. As depicted in Figure 9(a), this is the case when $T_{\mathrm{arr}} + T_B > T_{\mathrm{RT}}$. Since $T_{\mathrm{arr}} \sim \mathcal{U}(0, T_{\mathrm{RT}})$, on average $T_{\mathrm{arr}} = T_{\mathrm{RT}}/2$ and so the condition is:

$$T_{\mathrm{RT}}/2 + T_B > T_{\mathrm{RT}} \Longrightarrow T_{\mathrm{RT}} < 2T_B \tag{15}$$

Case 2: obstacle is no longer present, when the new RT is generated. As depicted in Figure 9(b), this is the case $T_{\mathrm{RT}} \geq 2T_B$. In this work, we just consider this option, otherwise the beam pair would be updated when the obstacle is still obstructing the best path, thus still reducing the average rate. Then, the rate R_{WB} experienced when reacting after the blockage is detected, by selecting a suboptimal solution in the RT instances, can be computed (for a fixed time window T_{RT}), as:

$$R_{\mathrm{WB}} = \frac{RT_{\mathrm{arr}} + rT_B + R(T_{\mathrm{RT}} - T_{\mathrm{arr}} - T_B)}{T_{\mathrm{RT}}} = \cdots = \frac{R(T_{\mathrm{RT}} - T_B) + rT_B}{T_{\mathrm{RT}}} \tag{16}$$

If no actions are taken, after the obstacle has been detected, the rate R_{OB} is:

$$R_{\mathrm{OB}} = \frac{RT_{\mathrm{arr}} + 0T_B + R(T_{\mathrm{RT}} - T_{\mathrm{arr}} - T_B)}{T_{\mathrm{RT}}} = \cdots = \frac{R(T_{\mathrm{RT}} - T_B)}{T_{\mathrm{RT}}} \tag{17}$$

The average rate gain (R_G) between the two options is:

$$R_G = \frac{R_{\mathrm{WB}}}{R_{\mathrm{OB}}} = 1 + \frac{r}{R} \cdot \frac{T_B}{T_{\mathrm{RT}} - T_B} \tag{18}$$

The factor r/R is the ratio between the average suboptimal rate perceived when selecting the second best beam pair in the RT, and the average optimal rate, when no obstacle was present in the path, respectively. This ratio depends on the mmWave BS density D and the number of antenna elements at the UE and BS sides.

This rate gain R_G has been simulated by placing an obstacle between the UE and its serving SCell and evaluating the average throughput experienced when the backup solution is set and then

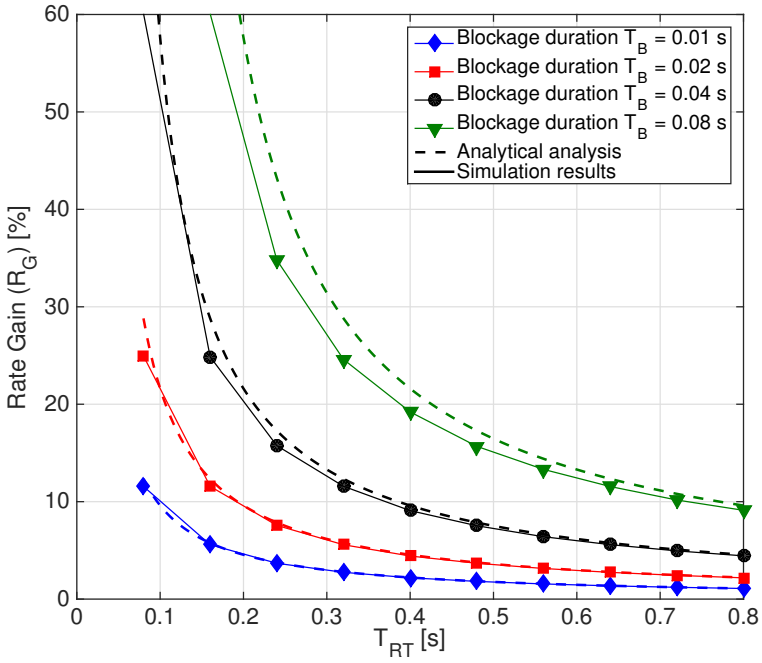

Figure 10: Percentage of rate gain R_G vs. RT periodicity T_{RT}, for different values of blockage duration T_B. The mmWave BS density is $D = 80$ BS/km^2. Dashed lines refer to the analytical expression in Equation (18). The simulation results asymptotically overlap with the theoretical curves. We just consider the case $T_{\mathrm{RT}} \geq 2T_B$.

no actions are instead taken. In Figure 10, when T_{RT} is sufficiently large, so when $T_{RT} \gg 2T_B$, the simulation curves asymptotically overlap with the dashed lines plotting Equation (18), for different values of D (determining different values of the ratio r/R).

Figure 10 shows that, for a fixed blockage duration T_B, as T_{RT} increases, the rate gain R_G decreases. In fact the portion of time in which the user would experience zero gain (if no actions are taken when the primary path is obstructed) proportionally decreases within the time window of length T_{RT}, making it less convenient to select a backup beam pair to overcome the blockage issue. Of course, as pointed out in Section VI-A, we could consider more frequent report tables (by reducing T_{RT}), to increase the average throughput of the network and R_G . However, this would lead to an increased overhead too, which would raise the system cost and complexity[6].

Moreover we see that, when T_B increases, the rate gain R_G increases as well, due to the increased enhancement provided by the use of a suboptimal beam pair after a blockage event

[6]We recall that, if we instead increase T_{RT} to reduce the overhead of the network, we further reduce the system throughput due to the variations and perturbation that may affect the mmWave channel, as shown in Section VI-A.

occurs, with respect to the baseline algorithm in which no actions are taken till the reception of a RT. Actually the blockage has longer duration and so the portion of time in which the network would have had zero rate, within a fixed time window T_{RT}, is more dominant.

VII. Conclusions and Future Work

A challenge for the feasibility of a 5G mmWave system is the high susceptibility to blocking that affects links in mmWave networks and results in rapid channel dynamics. In order to deal with these channel variations, a periodical directional sweep should be performed, to constantly monitor the directions of transmission of each potential link and to adapt the beam steering when a power signal drop is detected. In this work, we have proposed a novel measurement reporting system that allows a supervising centralized entity, such as the macro base station, operating in the legacy band, to periodically collect multiple reports on the overall channel propagation conditions, that can be used to make proper network decisions when implementing multiple control-plane features, such as initial access, handover, beam tracking and obstacle reaction. We argue that this proposed approach, which is based on uplink rather than downlink signals, can enable much more rapid and robust tracking and efficient and fair user association, enabling also the use of digital beamforming architectures to dramatically reduce the measurement reporting delay.

As part of our future work, we will design control applications that monitor and keep memory of the received signal strength variance, to better capture the dynamics of the channel and bias the cell selection strategy of delay-sensitive applications towards more robust cells. Moreover, a study on the implementation of analog, hybrid or fully digital beamforming architectures for such control procedures and a comparison among them deserve a deeper investigation.

References

[1] S. Rangan, T. S. Rappaport, and E. Erkip, "Millimeter-wave cellular wireless networks: Potentials and challenges," *Proceedings of the IEEE*, vol. 102, no. 3, pp. 366–385, March 2014.

[2] M. R. Akdeniz, Y. Liu, M. K. Samimi, S. Sun, S. Rangan, T. S. Rappaport, and E. Erkip, "Millimeter wave channel modeling and cellular capacity evaluation," *IEEE Journal on Selected Areas in Communications*, vol. 32, no. 6, pp. 1164–1179, June 2014.

[3] J. Lu, D. Steinbach, P. Cabrol, and P. Pietraski, "Modeling the impact of human blockers in millimeter wave radio links," *ZTE Commun. Mag*, vol. 10, no. 4, pp. 23–28, 2012.

[4] F. B. Tesema, A. Awada, I. Viering, M. Simsek, and G. P. Fettweis, "Mobility modeling and performance evaluation of multi-connectivity in 5G intra-frequency networks," in *IEEE Globecom Workshops (GC Wkshps)*, Dec 2015.

[5] Ericsson, *Microwave Towards 2020*, Sep 2015, Report. [Online]. Available: http://www.ericsson.com/res/docs/2015/microwave-2020-report.pdf

[6] K. Haneda, L. Tian, H. Asplund, J. Li, Y. Wang, D. Steer, C. Li, T. Balercia, S. Lee, Y. Kim, A. Ghosh, T. Thomas, T. Nakamurai, Y. Kakishima, T. Imai, H. Papadopoulas, T. S. Rappaport, G. R. MacCartney, M. K. Samimi, S. Sun, O. Koymen, S. Hur, J. Park, J. Zhang, E. Mellios, A. F. Molisch, S. S. Ghassamzadeh, and A. Ghosh, "Indoor 5G 3GPP-like channel models for office and shopping mall environments," in *IEEE International Conference on Communications Workshops (ICC)*, May 2016, pp. 694–699.

[7] C. N. Barati, S. A. Hosseini, M. Mezzavilla, P. Amiri-Eliasi, S. Rangan, T. Korakis, S. S. Panwar, and M. Zorzi, "Directional initial access for millimeter wave cellular systems," in *49th Asilomar Conference on Signals, Systems and Computers*, Nov 2015, pp. 307–311, *CoRR,* vol. abs/1511.06483. [Online]. Available: http://arxiv.org/abs/1511.06483

[8] M. Giordani, M. Mezzavilla, A. Dhananjay, S. Rangan, and M. Zorzi, "Channel dynamics and SNR tracking in millimeter wave cellular systems," in *European Wireless 2016 (EW2016)*, Oulu, Finland, May 2016, pp. 306–313.

[9] M. Giordani, M. Mezzavilla, S. Rangan, and M. Zorzi, "Multi-Connectivity in 5G mmwave cellular networks," in *15th Annual Mediterranean Ad Hoc Networking Workshop (Med-Hoc-Net'16)*, Vilanova i la Geltr, Barcelona, Spain, Jun. 2016.

[10] H. Shokri-Ghadikolaei, C. Fischione, G. Fodor, P. Popovski, and M. Zorzi, "Millimeter wave cellular networks: A MAC layer perspective," *IEEE Transactions on Communications*, vol. 63, no. 10, pp. 3437–3458, Oct 2015.

[11] S. Schwarz, C. Mehlfhrer, and M. Rupp, "Calculation of the spatial preprocessing and link adaption feedback for 3GPP UMTS/LTE," in *6th Conference on Wireless Advanced (WiAD)*, June 2010.

[12] 3GPP, "Technical specification group radio access network; Study on small cell enhancement for (E-UTRA) and (e-TRAN); Higher layer aspects (Release 12)," *TR 36.842*, 2013.

[13] A. Zakrzewska, D. Lopez-Perez, S. Kucera, and H. Claussen, "Dual connectivity in LTE HetNets with split control- and user-plane," in *IEEE Globecom Workshops (GC Wkshps)*, Dec 2013, pp. 391–396.

[14] Z. He, S. Mao, and T. T. S. Rappaport, "Minimum time length link scheduling under blockage and interference in 60 GHz networks," in *IEEE Wireless Communications and Networking Conference (WCNC)*, March 2015, pp. 837–842.

[15] V. Yazici, U. C. Kozat, and M. O. Sunay, "A new control plane for 5G network architecture with a case study on unified handoff, mobility, and routing management," *IEEE Communications Magazine*, vol. 52, no. 11, pp. 76–85, Nov 2014.

[16] S. Sesia, I. Toufik, and M. Baker, *LTE, The UMTS Long Term Evolution: From Theory to Practice*. Wiley Publishing, 2009.

[17] A. Talukdar, M. Cudak, and A. Ghosh, "Handoff rates for millimeterwave 5G systems," in *IEEE 79th Vehicular Technology Conference (VTC Spring)*, May 2014.

[18] H. Song, X. Fang, and L. Yan, "Handover scheme for 5G C/U plane split heterogeneous network in high-speed railway," *IEEE Transactions on Vehicular Technology*, vol. 63, no. 9, pp. 4633–4646, Nov 2014.

[19] S. Sadr and R. S. Adve, "Handoff rate and coverage analysis in multi-tier heterogeneous networks," *IEEE Transactions on Wireless Communications*, vol. 14, no. 5, pp. 2626–2638, May 2015.

[20] P. Coucheney, E. Hyon, and J. M. Kelif, "Mobile association problem in heterogenous wireless networks with mobility," in *IEEE 24th Annual International Symposium on Personal, Indoor, and Mobile Radio Communications (PIMRC)*, Sept 2013, pp. 3129–3133.

[21] C. N. Barati, S. A. Hosseini, S. Rangan, P. Liu, T. Korakis, S. S. Panwar, and T. S. Rappaport, "Directional cell discovery

in millimeter wave cellular networks," *IEEE Transactions on Wireless Communications*, vol. 14, no. 12, pp. 6664–6678, Dec 2015.

[22] A. Capone, I. Filippini, and V. Sciancalepore, "Context information for fast cell discovery in mm-Wave 5G networks," in *Proceedings of 21th European Wireless Conference*, May 2015.

[23] V. Desai, L. Krzymien, P. Sartori, W. Xiao, A. Soong, and A. Alkhateeb, "Initial beamforming for mmWave communications," in *48th Asilomar Conference on Signals, Systems and Computers*, Nov 2014, pp. 1926–1930.

[24] M. Giordani, M. Mezzavilla, C. N. Barati Nt., S. Rangan, and M. Zorzi, "Comparative analysis of initial access techniques in 5G mmwave cellular networks," in *Annual Conference on Information Science and Systems (CISS)*, Princeton, USA, 2016.

[25] M. Giordani, M. Mezzavilla, and M. Zorzi, "Initial access in 5G mm-Wave cellular networks," *CoRR*, vol. abs/1602.07731, 2016. [Online]. Available: http://arxiv.org/abs/1602.07731

[26] T. S. Rappaport, R. W. Heath Jr, R. C. Daniels, and J. N. Murdock, *Millimeter wave wireless communications*. Pearson Education, 2014.

[27] N. Moraitis and P. Constantinou, "Indoor channel measurements and characterization at 60 GHz for wireless local area network applications," *IEEE Transactions on Antennas and Propagation*, vol. 52, no. 12, pp. 3180–3189, Dec 2004.

[28] T. Nitsche, A. B. Flores, E. W. Knightly, and J. Widmer, "Steering with eyes closed: Mm-wave beam steering without in-band measurement," in *IEEE Conference on Computer Communications (INFOCOM)*, April 2015, pp. 2416–2424.

[29] A. Patra, L. Simic, and P. Mahonen, "Smart mm-wave beam steering algorithm for fast link re-establishment under node mobility in 60 GHz indoor WLANs." in *MobiWac*, 2015, pp. 53–62.

[30] S. Ferrante, T. Deng, R. Pragada, and D. Cohen, "mmWave initial cell search analysis under UE rotational motion," in *IEEE International Conference on Ubiquitous Wireless Broadband (ICUWB)*, Oct 2015.

[31] M. K. Samimi and T. S. Rappaport, "3-D statistical channel model for millimeter-wave outdoor mobile broadband communications," in *Proc. ICC*, June 2015, pp. 2430–2436.

[32] T. Bai and R. W. Heath, "Coverage and rate analysis for millimeter-wave cellular networks," *IEEE Transactions on Wireless Communications*, vol. 14, no. 2, pp. 1100–1114, Feb 2015.